

On nonlinear distortions of highly dispersive optical coherent systems

Francesco Vacondio,^{1,*} Olivier Rival,¹ Christian Simonneau,¹ Edouard Grellier,¹
Alberto Bononi,² Laurence Lorcy,¹ Jean-Christophe Antona,¹ and Sébastien Bigo¹

¹Alcatel-Lucent Bell Labs, Route de Villejust, 91620, Nozay, France

²Dipartimento di Ingegneria dell'Informazione, Università degli Studi di Parma, Italy

*francesco.vacondio@alcatel-lucent.com

Abstract: We investigate via experiments and simulations the statistical properties and the accumulation of nonlinear transmission impairments in coherent systems without optical dispersion compensation. We experimentally show that signal distortion due to Kerr nonlinearity can be modeled as additive Gaussian noise, and we demonstrate that its variance has a supra-linear dependence on propagation distance for 100 Gb/s transmissions over both low dispersion and standard single mode fiber. We propose a simple empirical model to account for linear and nonlinear noise accumulation, and to predict system performance for a wide range of distances, signal powers and optical noise levels.

©2012 Optical Society of America

OCIS codes: (060.1660) Coherent communications; (060.4370) Nonlinear optics, fibers.

References and links

1. A. Carena, G. Bosco, V. Curri, P. Poggiolini, M. T. Taiba, and F. Forghieri, "Statistical characterization of PM-QPSK signals after propagation in uncompensated fiber links," in Proc. ECOC 2010, paper P4.07 (2010).
2. E. Grellier and A. Bononi, "Quality parameter for coherent transmissions with gaussian-distributed nonlinear noise," *Opt. Express* **19**(13), 12781–12788 (2011).
3. G. Bosco, A. Carena, R. Cigliutti, V. Curri, P. Poggiolini, and F. Forghieri, "Performance prediction for WDM PM-QPSK transmission over uncompensated links", in Proc. OFC 2011, paper OTh07 (2011).
4. P. Poggiolini, A. Carena, V. Curri, G. Bosco, and F. Forghieri, "Analytical modeling of nonlinear propagation in uncompensated optical transmission links," *IEEE Photon. Technol. Lett.* **23**(11), 742–744 (2011).
5. A. Bononi, E. Grellier, P. Serena, N. Rossi, and F. Vacondio, "Modeling nonlinearity in coherent transmissions with dominant interpulse-four-wave-mixing," in Proc. ECOC 2011, paper We.7.b.2 (2011).
6. S. J. Savory, "Digital filters for coherent optical receivers," *Opt. Express* **16**(2), 804–817 (2008).
7. F. Forghieri, R. W. Tkach, and D. L. Favin, "Simple model of optical amplifier chains to evaluate penalties in WDM systems," *J. Lightwave Technol.* **16**(9), 1570–1576 (1998).
8. E. Torrenco, R. Cigliutti, G. Bosco, A. Carena, V. Curri, P. Poggiolini, A. Nespola, D. Zeolla, and F. Forghieri, "Experimental validation of an analytical model for nonlinear propagation in uncompensated optical links," in Proc. ECOC 2011, paper We.7.B.2 (2011).
9. D. Saha and T. G. Birdsall, "Quadrature-quadrature phase-shift keying," *IEEE Trans. Commun.* **37**(5), 437–448 (1989).
10. J. J. Filliben, "The probability plot correlation coefficient test for normality," *Technometrics* **17**(1), 111–117 (1975).
11. S. W. Looney and T. R. Gullledge, "Use of the correlation coefficient with normal probability plots," *Am. Stat.* **39**(1), 75–79 (1985).
12. E. Grellier, J.-C. Antona, and S. Bigo, "Global criteria to account for tolerance to nonlinearities of highly dispersive systems," *IEEE Photon. Technol. Lett.* **22**(10), 685–687 (2010).
13. A. Bononi, P. Serena, N. Rossi, and D. Sperti, "Which is the dominant nonlinearity in long-haul PDM-QPSK coherent transmissions?" in Proc. ECOC 2010, paper Th10E1 (2010).
14. A. Bononi, N. Rossi, and P. Serena, "Transmission limitations due to fiber nonlinearity," in Proc. OFC 2011, paper OWO7 (2011).

1. Introduction

The objective of this paper is to investigate the statistical nature of distortions induced by nonlinear effects, and to clarify how such distortions accumulate with distance in coherent systems with no optical dispersion management (NDM), for both standard single mode fiber (SSMF) and nonzero dispersion shifted fiber (NZDSF). We first experimentally assess the

behavior of a complete wavelength division multiplexed (WDM) 100 Gb/s polarization division multiplexed (PDM) quadrature phase shift keying (QPSK) system over a 50-GHz grid, including all propagation impairments, transmitter and receiver imperfections, and realistic digital signal processing. In this scenario, we experimentally confirm that an additive Gaussian noise channel can very well approximate the fiber channel both in linear and nonlinear propagation regimes [1]. We experimentally show the precision of a recently proposed analytical model [2–5] for evaluating the performance of such systems at a fixed propagation distance, and the dependence of nonlinear noise variance to channel power. We then demonstrate that for both SSMF and NZDSF the nonlinear noise variance has a faster-than-linear dependence on propagation distance. We propose a model accounting for this dependence and assess its precision in predicting performance for a wide range of propagation distances. Finally, we turn to simulations to gain further insight into the mechanism responsible for the accumulation of nonlinear distortions in the propagation of a WDM-PDM-QPSK signal at 100 Gb/s over a 50-GHz grid. We show the impact of the cumulated dispersion at the input of each span on the total nonlinear variance, and its importance on the overall supra-linear accumulation of nonlinear distortions.

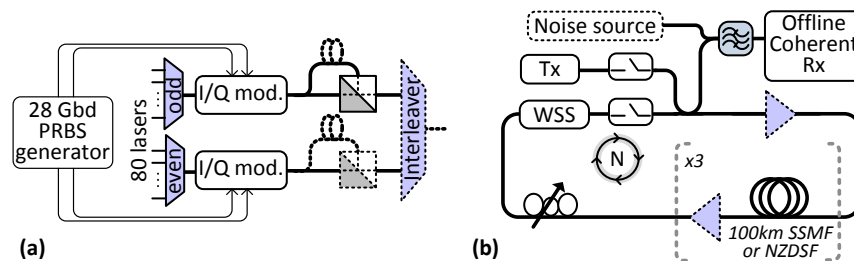


Fig. 1. Experimental setup of (a) transmitter and (b) recirculating loop.

2. Experimental setup

We investigate the respective impact of amplified spontaneous emission (ASE) noise and Kerr nonlinear distortion in a recirculating loop testbed. Figure 1(a) depicts the setup of the transmitter used in the experiment. Two combs of 40 lasers spaced by 100 GHz are independently modulated with I/Q modulators. The I/Q modulators are driven with 28 Gbaud pseudo random bit sequences (PRBS) of length $2^{15}-1$. As is customary in laboratory experiments, polarization division multiplexing is emulated by splitting the signal, delaying one branch, and recombining the signal through a polarization beam combiner. Finally, the two combs are combined using an interleaver to form a single WDM comb of 50GHz-spaced PDM-QPSK signals at 112 Gb/s, accounting for the transport of a 100Gb/s payload with 12% overhead for forward error correction and framing purposes. The experimental setup of the recirculating loop is depicted in Fig. 1(b). Inside the loop, light propagates into three spans of 100 km of either SSMF or NZDSF separated by erbium doped fiber amplifiers (EDFAs). The loop also comprises a polarization scrambler and a wavelength selective switch (WSS) for channel power equalization.

At the loop output, we can load additional ASE noise through an optical noise source. The channel under test is selected with a passband optical filter, and enters a coherent receiver. The optical filter 3-dB bandwidth is 50 GHz, and its shape is close to a 3rd order supergaussian. In the receiver, the signal beats with a local oscillator in a dual polarization downconverter before being photodetected. Transmitter laser and local oscillator have the same nominal linewidth of 300 kHz. After photodetection, a 16 GHz, 50 Gsamples/s real time oscilloscope is used to capture traces which are then processed offline. In the offline digital signal processing (DSP), the following steps are applied to the signal: 1) Normalization and resampling to 2 samples/symbol, 2) Chromatic dispersion compensation, 3) Adaptive blind equalization with the constant modulus algorithm [6], 4) Phase and frequency estimation and correction [6], 5) Electrical signal to noise ratio (SNR) evaluation 6) Symbol identification,

bit error ratio (BER) evaluation, and conversion to Q^2 factor. The convergence parameter of the adaptive equalizer is 10^{-3} [5], and the number of taps in the phase estimation filter was optimized for each configuration.

Figure 2(a) shows with markers the measured electrical SNR in back to back at the decision gate (expressed in an equivalent two-sided bandwidth of 12.47 GHz) as function of the optical signal to noise ratio ($OSNR_{ASE}$) before the receiver, measured in 0.1 nm (equivalent to 12.47 GHz). Here and throughout the paper, the signal to noise ratio will be referred to the nominal 0.1 nm bandwidth. As it can be seen, the SNR clearly shows saturation for high values of $OSNR_{ASE}$, which is a signature of transceiver imperfections or in-band cross-talk. The SNR can therefore be well modeled as [7,8]:

$$1/SNR = 1/OSNR_{ASE} + K_{TRX} \quad (1)$$

where K_{TRX} is a suitable constant depending on the particular practical implementation of the transmitter and receiver. In our case, $K_{TRX} = 1/215$ yields very good fit with the measured data, as can be seen in Fig. 2(a). Therefore, given our transceiver, the maximum achievable electrical SNR at the decision gate is ~ 23 dB.

The bit error ratio can finally be calculated from the SNR (linear scale) as [9]:

$$BER = 0.5\text{erfc}(\sqrt{\eta \cdot SNR}) \quad (2)$$

where $\text{erfc}(\cdot)$ is the complementary error function, and η is a suitable constant accounting for all deviations of the receiver from the ideal matched filter. With an ideal receiver, η is the ratio of the noise single-sided bandwidth and the signal baud rate, *i.e.* $\eta = (12.47/2)/28 \approx 0.22$. In our case, $\eta = 0.2$ gives a very good fit with the measured data, as can be seen in Fig. 2(b). It is important to stress that here, and throughout the paper, the Q^2 factor is calculated from the measured bit error ratio as $Q^2 = 20\log_{10}(\sqrt{2} \text{erfcinv}(2 \cdot BER))$, where erfcinv is the inverse of the complementary error function.

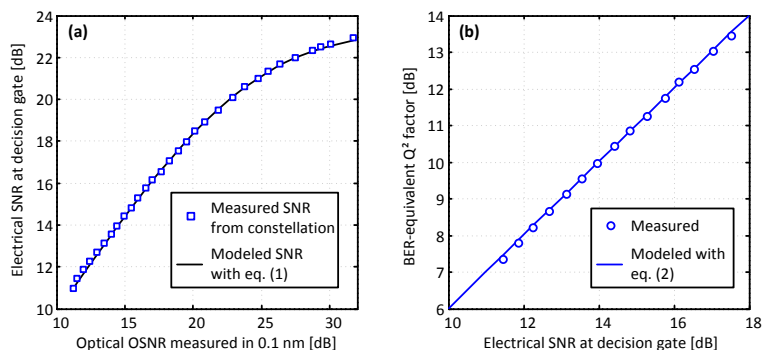


Fig. 2. (a) Back to back electrical SNR at the decision gate as function of the optical signal to noise ratio (b) Back to back BER-equivalent Q^2 factor as function of the electrical SNR at the decision gate.

3. Statistical characterization of measured signals after 15x100km of SSMF

In this section, we characterize the statistics of noise coming from ASE, nonlinear signal distortions, transmitter imperfections, all transmission impairments, and realistic receiver and digital signal processing. We measure the noise directly from the received QPSK constellation after propagation over 15x100 km of SSMF. As it is shown in Fig. 3(a), we identify the samples conditioned on the known transmitted symbols (different colors), we calculate their average (stars), which we will subtract from the signal, in order to remove modulation and obtain a zero-mean complex noise. We thoroughly tested the statistics of the noise for two exemplary channel powers: $P_L = -3$ dBm, and $P_H = +4$ dBm. Figure 3(b) shows the

measured OSNR_{ASE} at the receiver input as a function of power per channel after 15x100 km of SSMF propagation without additional noise loading. The noise figure of our EDFAs slightly varies with the optical power level at the amplifier input, therefore the measured OSNR_{ASE} deviates from the ideal 1 dB/dB law. As it can be seen, the OSNR_{ASE} at receiver input is 16 dB and 21.6 dB, for P_L and P_H respectively. These power levels have been chosen because they yield the same bit error ratio after transmission, but for the lowest power P_L the system is chiefly limited by OSNR_{ASE} , whereas for the highest power P_H the main source of impairments is fiber nonlinearity.

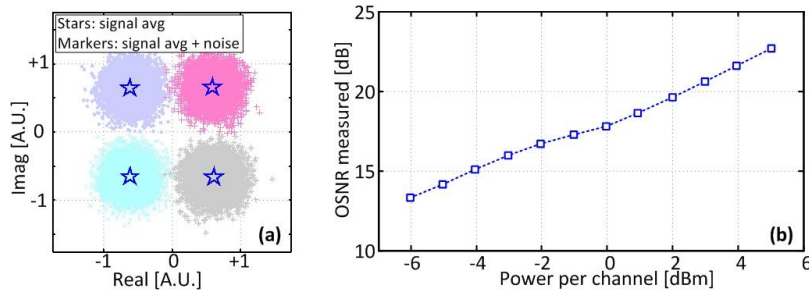


Fig. 3. (a) Typical measured QPSK constellation from which SNR and BER are measured (b) Measured OSNR_{ASE} in 0.1nm after 15 spans of SSMF, as a function of channel power (without noise loading).

To study the noise statistics, we have applied Filliben's probability plot correlation coefficient (PPCC) test for normality [10,11] to the measured signals. In this test, for each data set we calculate the correlation coefficient between the quantiles of the measured data and the quantiles of a theoretical Gaussian distribution. With a data set of size 1000 samples, when the correlation coefficient is on average higher than 0.9984 or 0.9979 (shown as red dashed lines in the plots) the hypothesis that the data is normal holds with more than 99% or 95% confidence, respectively. We have applied the test to more than 2500 different subsets of our signal, of size 1000 samples each (the test has been done independently for the real part and imaginary part of the recovered signal). Figure 4(a) and (b) shows the test results, for P_L and P_H respectively. In our case, the average PPCC is well above the 99% confidence level, therefore proving that for both powers the noise statistics are indeed normal. In conclusion, noise can be considered Gaussian both in the linear and in the nonlinear regime, where the major sources of impairments are ASE noise and nonlinearity-induced signal distortions, respectively.

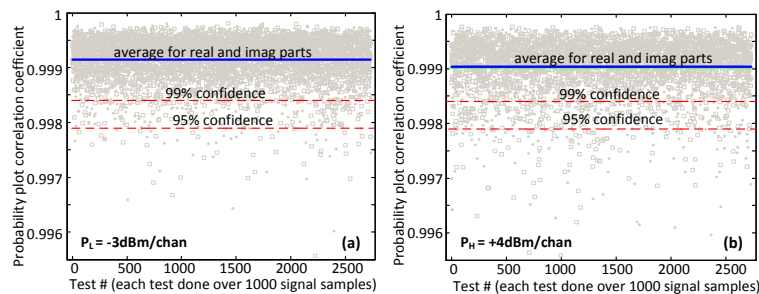


Fig. 4. Probability plot correlation coefficient for normality testing calculated over 1000 samples. The test is repeated more than 2500 times, and for real and imaginary parts. (a) $P_L = -3$ dBm (b) $P_H = +4$ dBm.

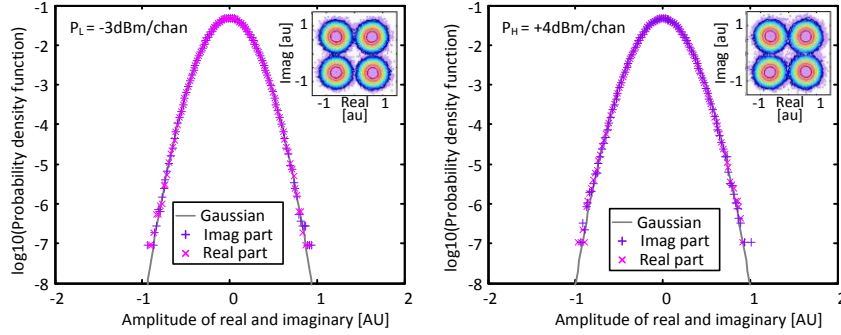


Fig. 5. PDF of real and imaginary components of total noise (markers: measured signals, line: theoretical Gaussian). Insets show an example of measured constellations. (a) $P_L = -3$ dBm (b) $P_H = +4$ dBm.

The normality of the noise is also visually confirmed by the excellent fit over more than 6 orders of magnitude of the probability density functions (PDFs) of real and imaginary part of the measured optical noise (markers) with a theoretical Gaussian PDF, shown in Fig. 5(a) for P_L and Fig. 5(b) for P_H . For these results, more than ten million measured samples have been used. The results shown here are for one polarization only, since for the other polarization the results are essentially identical: the normal hypothesis holds with more than 99% confidence, and the PDF fit is again very good. We can therefore conclude that in our transmission experiment noise is Gaussian and identically distributed in the 4D space of the two polarizations in-phase and quadrature components, both in the linear and nonlinear regimes.

4. Performance modeling and prediction at fixed distance

Recent works have proposed that the variance of the nonlinear noise for a given transmission link is well approximated as $a_{NL}P^3$, where P is the channel power and a_{NL} a suitable constant which depends on system parameters and can be obtained numerically, analytically, or by simple measurements [2–5]. The performance of the system can therefore be characterized by a “total” signal to noise ratio, which, adding the contribution of nonlinearities to Eq. (1), can be written as

$$1/\text{SNR}_{\text{tot}} = 1/\text{SNR}_{\text{lin}} + 1/\text{SNR}_{\text{NL}} \quad (3)$$

where $1/\text{SNR}_{\text{lin}} = (1/\text{OSNR}_{\text{ASE}} + K_{\text{TRX}})$ is the inverse of the linear part, and $1/\text{SNR}_{\text{NL}} = a_{NL}P^3/P$ is the inverse of the nonlinear signal to noise ratio, and thus depends on the channel power squared.

In this section we show how accurately Eq. (3) models system performance at a fixed distance. We experimentally measure the signal to noise ratio before the decision gate after 15x100km of SSMF propagation as a function of channel power, with and without additional ASE noise loading. From the measurement of the OSNR_{ASE} after propagation, together with the back to back characterization of K_{TRX} , we can infer SNR_{lin} . We can therefore obtain the signal to noise ratio due to nonlinearities SNR_{NL} from (3) and doing so, we have a method for separating the impact of linear noise due to ASE and transceiver imperfections from that of nonlinear noise coming from propagation distortions.

In Fig. 6(a) we report SNR_{tot} and its two components SNR_{lin} and SNR_{NL} as a function of signal power in the case of 15x100km of SSMF propagation without noise loading (empty markers). Filled markers are the result of a measurement where we load noise at the receiver, to degrade the OSNR_{ASE} by roughly 2 dB. Without noise loading, SNR_{tot} has a maximum at the optimal power per channel $P_{\text{NL,T}} \sim 1.5$ dBm (visualized by a vertical line in Fig. 6). The linear part SNR_{lin} increases as the signal power (and therefore the OSNR_{ASE}) grows. The nonlinear signal to noise ratio SNR_{NL} , on the other hand, decreases as the signal power triggers the nonlinear effects. As it can be seen, the measured SNR_{NL} has a slope of roughly -2

dB/dB, therefore confirming its dependence on $1/P^2$. The solid lines show the results of the model, where Eq. (3) has been used. In Eq. (3), we have used the measured $OSNR_{ASE}$, K_{TRX} as characterized in back to back, and $a_{NL} = 3.3e-3 \text{ mW}^{-2}$. The value of a_{NL} has been calculated from the measured value of SNR_{NL} in the case without noise loading, for the power $P = 4 \text{ dBm/chan}$, using $a_{NL} = 1/(SNR_{NL} \cdot P^2)$. The same value of a_{NL} is used also in the second series of measurements. The model in both cases fits very well the measured values.

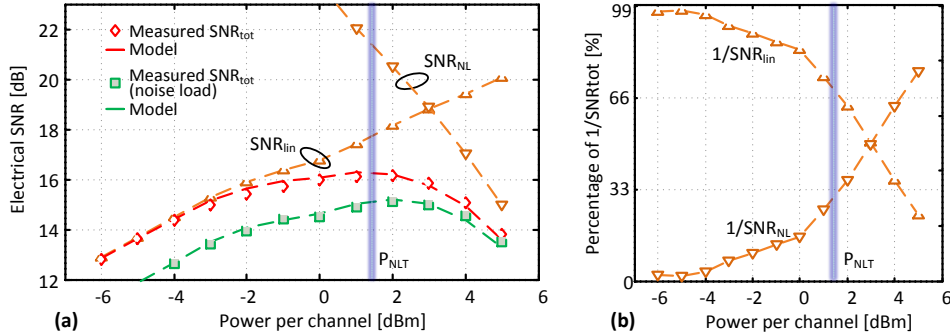


Fig. 6. (a) Measured and modeled total SNR after 15x100km SSMF transmission with and without noise loading versus channel power (b) $1/SNR_{in}$ and $1/SNR_{NL}$ are shown as percentage of the total $1/SNR$.

Figure 6(b) shows $1/SNR_{in}$ and $1/SNR_{NL}$ as fraction of $1/SNR_{tot}$, in the case without noise loading. Around P_{NLT} , the nonlinear noise power is half the linear noise power as predicted in [2,3], as $1/SNR_{NL}$ accounts for $\sim 33\%$ and $1/SNR_{in}$ for $\sim 66\%$ of the total noise-to-signal ratio.

Figure 7(a) shows the measured BER-equivalent Q^2 factor for the same system (markers). The modeled values obtained using (3) and (2), using the same a_{NL} value characterized before, are shown as solid lines. Figure 7(b) shows the error of the modeled Q^2 -factor with respect to the measured value, as function of the power per channel. As it can be seen, the error is always within $\pm 0.3 \text{ dB}$, indicating excellent agreement between model and measurements also for prediction of bit error ratio.

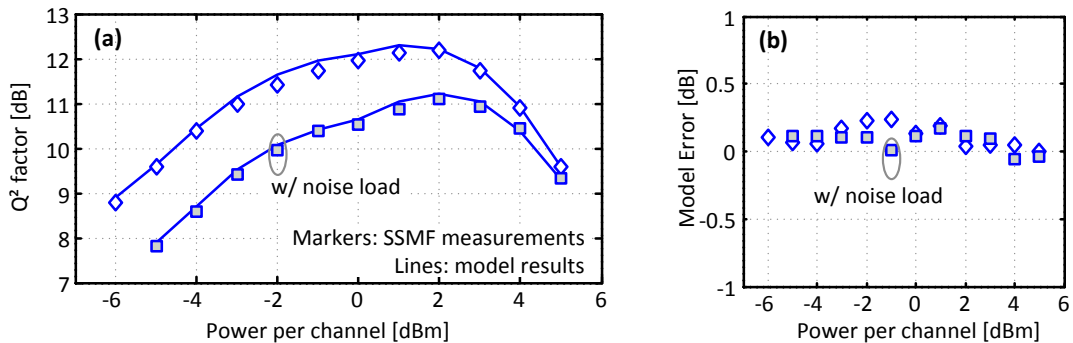


Fig. 7. (a) Q^2 factor versus power per channel for 15x100km SSMF transmission, with and without noise loading (Solid lines: model, markers: experiment). (b) Model error vs. power per channel.

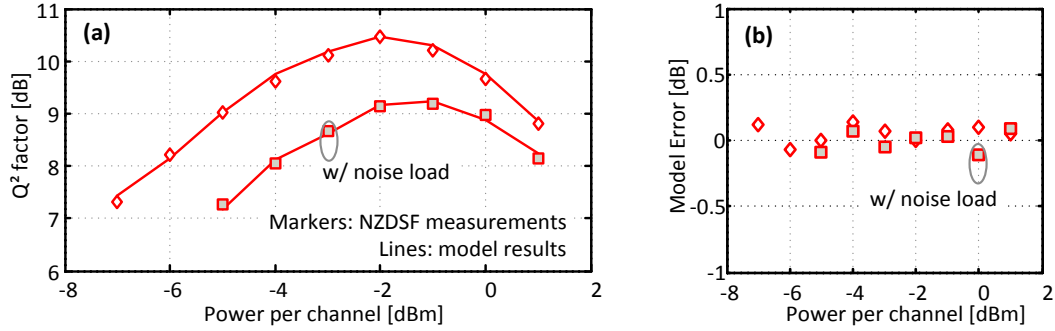


Fig. 8. (a) Q^2 factor versus power per channel for 15x100km NZDSF transmission, with and without noise loading (Solid lines: model, markers: experiment). (b) Model error vs. power per channel.

We have repeated the same experiment (15x100 km propagation) using nonzero dispersion shifted fiber instead of SSMF. The test channel was at 1546.12 nm, where the local dispersion is ~ 4 ps/nm/km. Figure 8(a) shows the modeled and measured Q^2 factor for this configuration, and Fig. 8(b) shows the model error. As compared to SSMF, there is a reduced tolerance to nonlinear effects, due to the lower local dispersion and effective area. Still, the model holds very well, yielding an error of the modeled Q^2 factor with respect to the measured one within ± 0.2 dB.

5. Performance modeling and prediction for variable distance

In this section, we use Eq. (3) to calculate $1/\text{SNR}_{\text{NL}}$ for a fixed power and variable number of spans, in order to investigate its dependence on propagation distance. In this configuration $1/\text{SNR}_{\text{NL}}$ is proportional to the nonlinear noise variance, so that we can use $1/\text{SNR}_{\text{NL}}$ to deduce rules on the accumulation of nonlinearity-induced distortions.

Figure 9(a) shows (for SSMF propagation) the values of $1/\text{SNR}_{\text{NL}}$ calculated with Eq. (3) from the measured data (electrical SNR, K_{TX} and OSNR_{ASE}) as function of the number of spans. We repeated the experiment for powers from +1 dBm/channel to +5 dBm/channel. The slope of the linear fit in log-log scale, shown with a solid line, is almost independent of the channel power. The average slope over the investigated powers and span range is 1.37 dB/dB. That means that the nonlinear noise variance grows as $\sim N^{1.37}$, where N is the number of spans. For NZDSF propagation, Fig. 9(b) shows the same type of results. Again, it can be seen that nonlinear noise accumulates almost independently of the power per channel, and the average slope is 1.33 dB/dB. Similarly to SSMF, the nonlinear noise variance therefore grows as $\sim N^{1.33}$.

Recalling from previous section that $1/\text{SNR}_{\text{NL}} = a_{\text{NL}}P^2$, our results therefore suggest that a_{NL} can be written as

$$a_{\text{NL}} = \alpha_{\text{NL}} N^{1+\varepsilon} \quad (4)$$

where α_{NL} is a constant which in turn does not depend on transmission distance, and the dependence on the number of spans is governed by the exponent $1 + \varepsilon$, where $\varepsilon = 0.37$ over SSMF and $\varepsilon = 0.33$ over NZDSF. Equation (4) is in line with [12], where authors show that in order to keep the same amount of nonlinearities for each span, the optical power should decrease as a certain power of the number of spans.

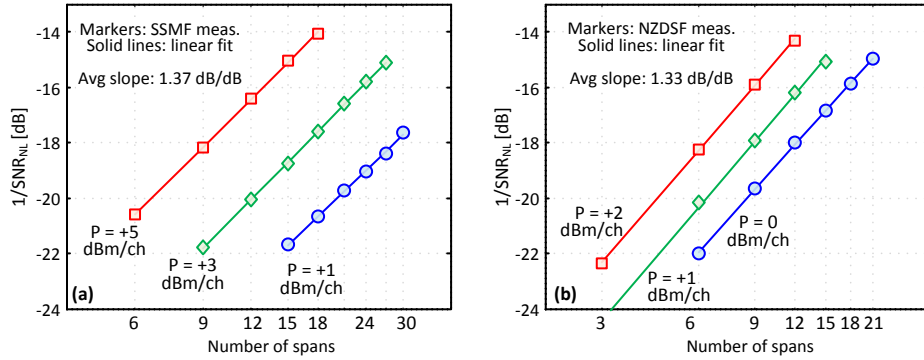


Fig. 9. $1/SNR_{NL}$ calculated from measurements for different channel powers as function of number of spans in dB scale. Solid lines are linear fit. Transmission over (a) SSMF, (b) NZDSF

Next, we use the new expression of Eq. (4) for a_{NL} in Eq. (3), and with Eq. (2) we predict system performance as function of distance. Results are shown in Fig. 10(a) for SSMF and Fig. 10(b) for NZDSF. In the figures, markers are experimental results of Q^2 factor versus propagation distance for different optical powers per channel. The solid lines show the results of the proposed model, where ε is used as calculated before. Once ε is determined, a single free parameter α_{NL} is needed for each fiber type, with which system performance can be predicted accurately for a wide range of distances, noise level and channel power. The single parameter actually depends on the characteristics of the optical fiber, as well as on the modulation format which is employed. As it can be seen, there is very good agreement of the model with the measured data.

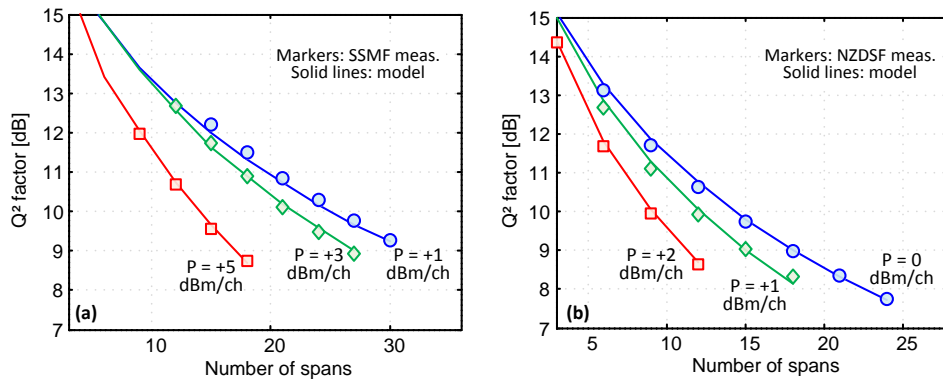


Fig. 10. Measured BER-equivalent Q^2 factor is shown as function of the number of spans in linear scale. Solid lines are the results of the model. Transmission over (a) SSMF, (b) NZDSF

One would be tempted to speculate that, in NDM systems, the contribution of each span to the total nonlinear noise would be independent of, or at least uncorrelated to, the contribution of the other spans, due to the large walk-off and pulse distortions induced by uncompensated chromatic dispersion. If that was the case, and if the same nonlinear noise was generated in each span, then the total nonlinear noise variance would be directly proportional to the number of spans N : with our formalism, that would mean $\varepsilon = 0$. On the contrary, our measurements suggest that, in the systems considered in this study, $\varepsilon > 0$. Next section will investigate numerically the origin and the nature of this non-trivial result.

6. Kerr effect-induced signal distortions accumulation

In our simulation setup, we consider 7 channels on a 50 GHz grid modulated with PDM-QPSK at 112 Gb/s. We use independent pseudo-random quaternary sequences of length 4096

symbols on the two polarizations of each channel. The channels states of polarization (SOPs) and relative delays are random. We do not take into account fiber polarization mode dispersion. Signal propagation is simulated by numerically solving the vector nonlinear Schrödinger equation through the split-step Fourier method with 2^{18} FFT points. The systems under test are based on 100-km spans of SSMF or NZDSF without optical dispersion compensation. The spans are separated by EDFAs which exactly compensate for the optical loss of the preceding fiber. The nonlinear interaction of ASE noise and signal is known to be negligible in NDM systems [13]; we therefore safely neglect ASE noise in our simulations. We are thus able to estimate the distortions induced by the sole Kerr effect by subtracting the (normalized) optical field launched into the transmission link from the (normalized) optical field at the link output. After having verified that the statistics of such distortions are well approximated by a Gaussian distribution (identically distributed in the 4D space of in-phase and quadrature components for the two polarizations), we express results in terms of the variance of this nonlinear noise.

Figure 11(a) shows the variance of the nonlinear noise, normalized to unit symbol power and calculated over 12.47 GHz, as function of the number of spans for SSMF at 1550 nm and NZDSF at 1550 nm and 1530 nm, assuming -3dBm channel power in all cases. The local dispersion is 17 ps/nm/km, 4.25 ps/nm/km and 2.5 ps/nm/km, respectively. The effective area is $80\ \mu\text{m}^2$ for SSMF, and $72\ \mu\text{m}^2$ for NZDSF. The loss coefficient is 0.22 dB/km for both SSMF and NZDSF. We repeated the simulation 20 times, randomly changing the channels SOPs, relative delays and sequences. These random parameters account for a $\sim 1\text{dB}$ spread in the variance of the nonlinear noise for a given fiber type and number of spans. At fixed number of spans still, the variance of nonlinear noise is found to increase from SSMF to NZDSF (1550nm) to NZDSF (1530nm).

For a given fiber type and wavelength, Fig. 10(a) shows that the variance of nonlinear noise versus span count can be approximated with excellent accuracy by a linear fit in dB/dB scale with a slope strictly greater than 1, confirming at least qualitatively the findings of the experimental results presented in section 5. Specifically, we find slopes of 1.18, 1.24 and 1.29 dB/dB for SSMF, NZDSF (1550nm) and NZDSF(1530nm). These values are somewhat lower than those found experimentally. The slight discrepancy is assigned to the presence of sources of impairments other than Kerr effect in the experimental setup (polarization dependent loss, imperfect DSP, ...)

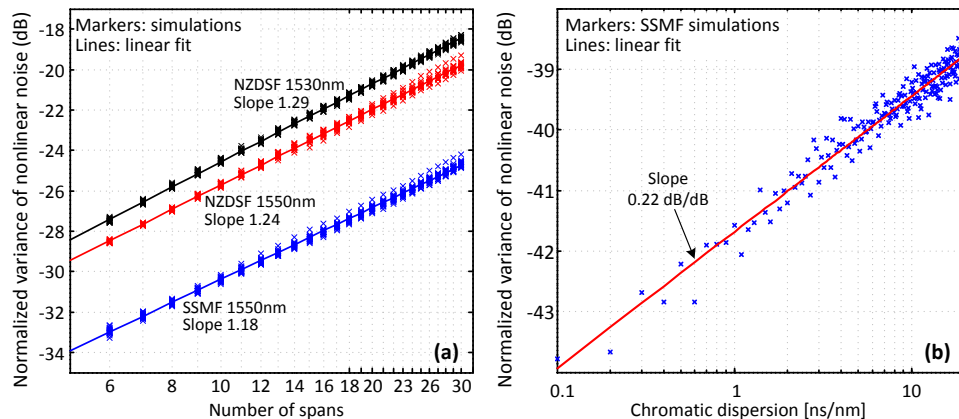


Fig. 11. Numerically calculated variance of nonlinear noise normalized to signal power (a) As function of the number of spans for NZDSF and SSMF, and (b) For a single span as function of chromatic dispersion at the input of the span.

This faster-than-linear growth of the variance of nonlinear distortions may have two (possibly combined) sources:

- Partial (positive) correlation, *i.e.*, constructive interference, between the distortions induced by different spans of the transmission links. In the extreme case of all spans creating an identical distortion f , the total distortion after N spans would be Nf and its variance $N^2\text{var}(f)$, thus yielding a 2 dB/dB growth of the total variance of nonlinear distortion with the number of span.
- Increasing of the noise variance generated by the individual spans along propagation, *i.e.*, each span generates a nonlinear noise, the variance of which is greater than the variance generated by the preceding span.

In order to test the latter hypothesis, we present in Fig. 11(b) the variance of the nonlinear distortion created by a single span of 100 km of SSMF with 0 dBm channel power as a function of the cumulated chromatic dispersion at the span input. Besides some scatter (due to random realizations of channels sequences, SOP and delays) a clear linear growth of the variance of nonlinear distortions versus chromatic dispersion in dB/dB scale can be observed. Denoting the average slope ζ , we find $\zeta \sim 0.22$. This result agrees with the intuition that in NDM links, chromatic dispersion gradually distorts the optical signal, increasing the occurrence of short power spikes prone to high nonlinear distortions and increasing the number of interpulse four wave mixing interactions.

Assuming complete decorrelation between spans, the variance of the total nonlinear distortion f_{tot} can be written as the sum of the variance of f_k^2 s, where f_k is the nonlinear distortion induced by the span k . Grouping the various results presented in this paper, we can write $\text{var}(f_k)$ as:

$$\text{var}(f_k) = AP^3 C_k^\xi \quad (5)$$

where P is the channel power, C_k the cumulated chromatic dispersion at the input of span k and A is a constant which is independent of the channel power and propagated distance. This model clearly fails for the first span of a transmission link without precompensation, as the zero chromatic dispersion at the span input would yield zero nonlinear distortion regardless of the power. Keeping in mind that the first span must be handled separately, the variance of the total nonlinear distortions can thus be written as:

$$\text{var}(f_{tot}) = \text{var}(f_1) + \sum_{k=2}^N AP^3 C_k^\xi = A_1 P^3 + AP^3 D^\xi L_{span}^\xi \sum_{k=2}^N (k-1)^\xi \approx A_1 P^3 + \frac{AP^3 D^\xi L_{span}^\xi}{1+\xi} (N-1)^{1+\xi} \quad (6)$$

where A_1 is a constant to account for the first span noise variance $\text{var}(f_1)$, D is the local chromatic dispersion, L_{span} is the span length, and we have used $C_k = DL_{span}(k-1)$, assuming that all spans are of equal length.

The right hand side expression in Eq. (6) is obtained through approximation of the discrete sum over the number of spans by the corresponding integral. For N large enough, we thus find $\text{var}(f_{tot}) \propto N^{1+\xi}$ with $1 + \xi = 1.22$. This value is very close to the 1.18dB/dB slope found in Fig. 11(a) for SSMF links and the small remaining discrepancy is within the accuracy of the simulation. We have thus proved that the variance growth versus span number in NDM systems is mostly to be attributed to the increase of per-span variance according to the empirical law (5), rather than to correlations among spans.

In [4], authors investigate a Nyquist-WDM system, where the channel spacing is equal to the baud rate. They report a linear growth of the nonlinear variance with the number of spans, whereas we report a supra-linear growth. In our system, self phase modulation is known to dominate over cross nonlinear effects [14]. At the Nyquist limit, as in [4], cross channel effects are stronger, due to the reduced channel spacing. It is therefore reasonable to speculate that intrachannel effects induce a faster growth of the nonlinear variance with respect to interchannel effects, and this will be the object of a separate study.

7. Conclusion

We have experimentally shown that, in the case of a 50-GHz-spaced WDM-PDM-QPSK 100 Gb/s transmission system without optical dispersion compensation, the optical fiber channel can be modeled by an additive Gaussian noise channel with high accuracy. We characterized the noise variance with respect to signal power, ASE level and distance. We proposed a simple empirical model to account for the distance dependence of the nonlinear noise variance, which is shown to be able to predict Q^2 factor with accuracy within ± 0.3 dB over a wide range of distances.

Via simulations we have investigated the nature of nonlinear distortions accumulation, showing that not all spans contribute equally to the total nonlinear noise variance, since the nonlinear noise generated in a span is a function of the chromatic dispersion at the span input. Finally, we have shown that a simple model assuming uncorrelated per-span nonlinear distortions whose variance grows as in (5) reasonably justifies (with an error which is within simulation accuracy) the observed variance growth.

Acknowledgments

Authors acknowledge partial funding from French project 100GRIA, and from the Celtic project EO-Net.